Flexural properties of concrete beams reinforced with UCAS

Toshiaki OHTA *, Rudy DJAMALUDDIN**,
Shinichi HINO***, Kohei YAMAGUCHI**** and Koji HARADA*****

* Dr.Eng., Professor, Dept. of Civil Engineering, Kyushu University, Fukuoka
** M.Eng., Graduate student, Dept. of Civil Engineering, Kyushu University, Fukuoka
*** Dr.Eng., Associate Prof., Dept of Civil Engingeering, Kyushu University, Fukuoka
**** Dr.Eng., Asistant, Dept of Civil Engingeering, Kyushu University, Fukuoka
***** Dr.Eng., Nishimatsu Construction Co., Ltd., Chuo-Ku, Fukuoka

UCAS, as an abbreviation from Unresin Carbon-fibers Assembly System, is a new system in applying of carbon fibers material as reinforcement for concrete structures. In UCAS, the carbon fiber is applied as reinforcement without impregnating them with resin. By this method, cables made of UCCF with a tensile strength of more than 1.4 GPa may be achieved. In order to clarify the performance of the concrete beam reinforced by UCAS, an experimental investigation has been done and the results of this study are presented in this paper. In addition, a grid system is considered herein to obtain the role of mechanical bonding like on the usual steel reinforcement. The results indicate that, the capacity of concrete beam reinforced by UCAS method could be controlled by bond capacity of grids. The beams that fail earlier under grid-bond failure show the pseudo-ductile performance. Finally, the results indicate that UCAS could be a good alternative for reinforcement of concrete structure members.

Keywords: *Carbon fibers, Flexural behavior, Grid, Bond capacity*

1. Introduction

Concrete and reinforced concrete are used as building materials in every country. Steel reinforced concrete is a dominant structural material in engineered construction. For more than a century it has been playing a key role in the building of modern architecture and social infrastructure [1]. Unfortunately, for structure in extremely aggressive environments, corrosion of the steel can be a significant problem [2),3),4)]. Furthermore, in modern times when structures are being built densely in larger numbers, the construction of good-quality reinforced concrete structures is becoming difficult especially in Japan where the use of sea sand is inevitable and skilled workers have been decreasing [1]. Many approaches are being tried to inhibit the corrosion mechanism in aggressive environments. One alternative approach being developed worldwide at an increasing pace is the replacement of the steel by continuous fibers such as carbon, glass or aramid. Usually, the fibers are encased in a resin to form a FRP composite [5),6)].

In other side, in 21st century society also known as the IT era, the information technology (IT) has been rapidly changing worldwide social and economic systems. In Japan, the information technology has been influencing every political and economic field and demanding structural changes [1]. By looking into the recent problems and demands of the 21st century then the keywords representing 21st century construction include digitalization, weight reduction, automation, size reduction, fast distribution, labor saving, corrosion resistance, recycling, and mechanical properties may be taken out.

Materials compatible with those keywords include carbon fibers, aramid fibers and polyethylene fibers. Carbon

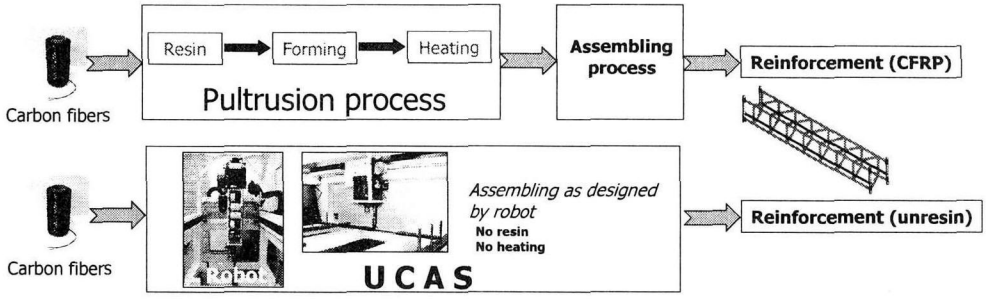

Figure 1 Pultrusion process vs UCAS

fibers are considered one of the most suitable in view of the strength, tensile modulus, resistance to corrosion, lightweight, creeping characteristics and fire resistance [1]. Usually, the unresin carbon fibers are impregnated into resin matrix to form rigid fiber reinforced plastics (FRP). The process in making of FRP is known as the pultrusion process.

In this paper, a new system in constructing a reinforcement system using unresin carbon fibers is introduced. The system is named UCAS (Unresin Carbon-fibers Assembly System). Figure 1 shows the pultrusion process vs UCAS. The merits of UCAS include economic advantage, lightweight, uncorrosive, high strength, and adaptability to IT era, etc.

In the pultrusion process, the reinforcing material such as carbon fiber filaments are pulled through a bath of thermoset resin, through forming guides and through a heated die to form a FRP. After traveling through the continuous process, the profiles are cut to the desired length with an abrasive saw or wheel. For using as reinforcement in a concrete structure, an assembling process is still needed. The hardware needed to process the carbon fibers in pultrusion process makes the product is still relatively expensive.

In UCAS, the unresin continuous carbon fibers (UCCF) string (Figure 2) supplied by a manufacturer company are used directly as reinforcement without impregnated into resin. The resin impregnation and thermosetting process are no need in UCAS. The assembling process of UCCF string to be an unresin reinforcing cable is done by an assembler robot. By this method, a reinforcement system is built as designed using the robot based on digitized design drawings. In assembling process, the carbon fibers are assembled under a certain tensile force. The production cost of reinforcement system constructed by UCAS can be reduced by eliminating some process such as impregnation and thermosetting process. Comparing with the pultrusion process, this new method is much cheaper[1]. The light weight of the reinforcement produced by UCAS method enables saving of heavy equipment including cranes, and increases the safety and efficiency of construction work. The partially unresin carbon fibers reinforcement system have been also considered in UCAS as an alternative for reinforcing system using the unresin carbon fibers. In this system, both the carbon fibers reinforced plastic (CFRP) and unresin reinforcing cables are used as reinforcement in reinforced concrete structures.

In this study, cables made from unresin continuous carbon fibers (UCCF) are applied to the concrete beam as tensile reinforcement. Experimental test[1] has shown that the strength of the final cable product is normally much lower than the strength of UCCF string itself. These cables have a tensile strength of approximately 35% of the nominal tensile strength of UCCF string as stated by the manufacturer [1]. This is attributed to the natural fact that it is impossible to initialize all strength of small fibers bundled into one cable. This is dominantly caused by the un-uniformness of initial stress of micro fibers. However, compare to steel reinforcement, these cables have much higher tensile strength than usual steel reinforcement and enough for applying as reinforcement material. Because the robot is still under development, some of process in this study are still done manually. The carbon fibers cables used in this study are made by the automatic reinforcement arrangement robot.

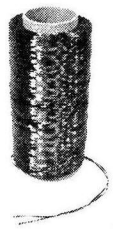

Figure 2 Unresin continuous carbon fibers (UCCF)

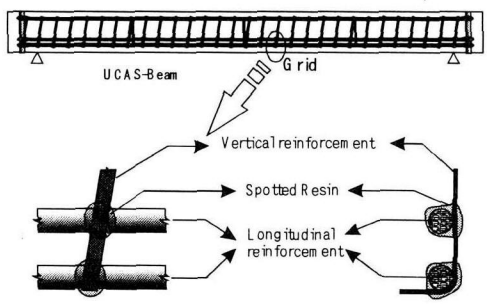

Figure 3 Detail of grid system

Table 1 List of specimens

Type	Specimen name		Reinforcement type [1]	Reinforcement						Expected Failure mode [4]
				Longitudinal			Vertical (stirrup)			
				No. of turning [2]	n x A(mm^2) [3]	Ratio (%)	(strings)	A(mm^2)	Pitch (mm)	
A	A-60	1 2 3	UCCF 12K	22	4 x 20.2	0.78	5	2.3	60	Compression
	A-40	1 2 3	UCCF 12K	22	4 x 20.2	0.78	3	1.4	40	Compression
B	B-60	1 2	UCCF 12K	17	4 x 16.5	0.61	5	2.3	60	Compression-Tensile
	B-40	1 2	UCCF 12K	17	4 x 15.6	0.61	3	1.4	40	Compression-Tensile
C	C-60	1 2	UCCF 12K	14	4 x12.9	0.49	5	2.3	60	Tensile

Notes: 1) 12K = 12,000 of fillament in one string
2) per one cable
3) n = Number of cables for tensile reinforcement
4) See also Table 3

Table 2 Material properties

Material name		Strength (Mpa)			Young modulus (Gpa)	Mass density (gr/cm^3)	Area (mm^2)
		Tensile	Compression	Shear			
UCCF 12K string [1)]		4800	-	-	230	1.82	0.46
Resin		29.4	68.6	9.8	-	-	-
Concrete	A-60	2.95	40.1	-	29.6	2.40	-
	A-40						
	B-60	3.24	46.3	-	35.5	2.40	-
	B-40						
	C-60						

Notes: 1) Provided by maker (nominal properties of Torayca-T700S) [8]

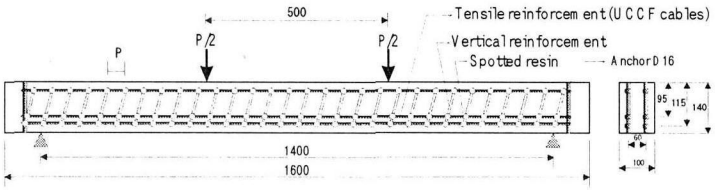

Figure 4 Detail of specimen

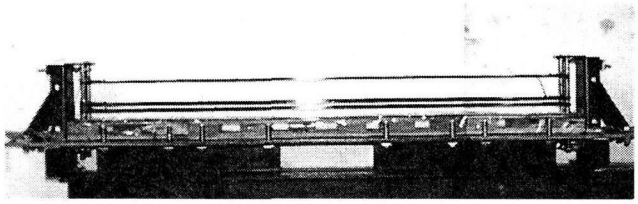

(a) Strengthened cables on special form work

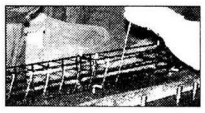

(b) Vertical reinforcement

(c) Jointing of intersection

Figure 5 Special form work and assembling process

As tensile reinforcement, it is necessary that the reinforcement bond to the concrete for an effective reinforcing action [4)], except in the special case of an unbonded tensile reinforcement system. Accordingly, a grid-system (Figure 3) has been developed on UCAS to create a mechanically bonding effect between longitudinal reinforcement and concrete. The grids are constructed by connecting the intersection points between a pair of longitudinal reinforcement and vertical reinforcement by epoxy resin.

This paper reports the result of a research program that investigates the behavior and capability of concrete beams reinforced by UCAS. For the investigation purposes, three types of concrete beam have been prepared and tested under flexural test as simple supported beam. The experimental results are analyzed to study the flexural properties of concrete beam reinforced by UCAS method.

2. Test Program

2.1 Test specimens and assembling process

To study the flexural behavior of concrete beam reinforced by this method, three types of concrete beam, as listed in Table 1, with span of 1400 mm have been constructed. The details of specimen are presented in Figure 4. The nominal reinforcement ratio of types A, B and C are 0.78%, 0.61% and 0.49%, respectively. All specimens were reinforced by four cables as tensile reinforcement. For vertical reinforcement turning purposes, two cables were also placed in compression section. The UCCF cables were assembled by assembler robot. The cables were made by turning UCCF string between two end-anchors as designed. The specimen types A, B and C consisted of 22, 17 and 14 turns for each cable, respectively. And then, the assembled cables were installed on the special steel mould that facilitates the strengthening of the cables under 800 N of tensile forces, as shown on Figure 5(a). Vertical reinforcement was constructed by turning the UCCF string helically covering the longitudinal reinforcements (Figure 5(b)). The grids were constructed by connecting the intersection points of a pair of longitudinal reinforcement and vertical reinforcement with epoxy resin (Figure 5(c)). Resin was allowed to harden before the concreting process. Resin can harden under room temperature in 24 hours. The beam specimens were remolded a day after concreting and cured in the curing room for 14 days. Material properties of UCCF string stated by manufacturer (designated name is Torayca-T700S)[8)], resin and concrete are shown in Table 2. Experimental test shows that the tensile strength of cables is about 35% of the tensile strength of UCCF string shown in Table 2 or 1680 MPa.

2.2 Test setup

In this study, all specimens were tested as simple

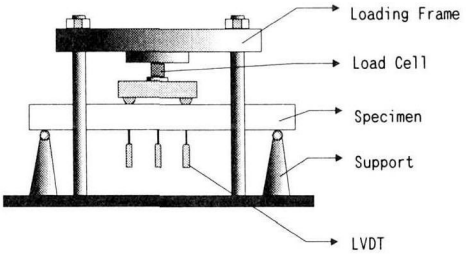

(a) Loading system

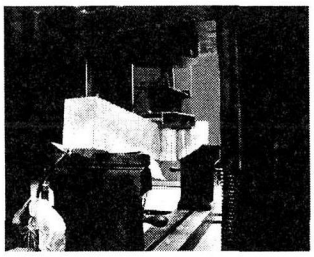

(b) Specimen under test

Figure 6 Test setup

supported beam with the span of 1400 mm. Each specimen was subjected to two equal static loads at the center of its span (Figure 6). The loading point distance was 500 mm. The beams were instrumented with three linear variable differential transformers (LVDTs) at mid-span and at the two loading points to monitor deflection. Also, strain gauges were bonded to the concrete surfaces, as well as on the reinforcement to measure the strain. The beams, spanning 1400 mm, were subjected to four-point flexural bending testing (pure bending) with a loading point distance of 500 mm. An automatic data acquisition system connected to a computer was used to monitor loading, as well as the deflection and strains in the concrete and reinforcement. The load was applied to the beam, step by step at a rate of 1 kN per step, by means of a hydraulic jack and was measured with a load cell. When flexural crack appeared, the crack width gauges were attached to measure the width of cracks. At the end of each step, cracks were sketched and measurements of deflection and strain reading were recorded for later processing. The test was stopped when deflection at mid-span reached 30 mm

3. Result and Discussion

3.1 Load-deflection response

Figures 7(a) and (b) show the load-deflection curves for the beams tested. Initially, the beams were un-cracked and stiff, like usual reinforced concrete beams. With further loading, cracking occurred at mid-span when the applied moment exceeds the cracking moment Mcr, causing a reduction in stiffness, which is greater for the specimens with lower reinforcement ratio. This can be attributed to the fact that crack width are bigger and crack spacing narrower in specimens with lower reinforcement ratio. From here, the load was still increasing followed by crack widening and the appearance of new cracks. The over opening of one crack can be avoided because of the existence of grids. The load-deflection curve for this step was almost linear until the concrete compressive zone started to deteriorate. On the specimen A-60 and A-40, the crushing of concrete at compression side led to a sudden decrease in load capacity with almost no change in deflection. From here, the beams enter into the next condition where deflection increases with little change in load until the end of test. This condition is called "second stable condition". As it can be observed that the second stable condition occurred at load level approximately 50% of maximum load. On the specimens B-60, B-40, and C-60, it was found that the grid failed earlier before the concrete crushed. This phenomenon was visually observed which was indicated by suddenly opening of one crack. This caused the crack to open fast and go upwards reducing the compressive zone and then was followed by the crushing of concrete. From here, the load did not drop significantly as for the specimen type A, but the deflection increased with little change in load and showed pseudo-ductile behavior. On the specimen C-60 with lowest reinforcement ratio, the crushing of concrete occurred soon after grid broken. This can be attributed to the fact that crack openings are wider in specimens with lower reinforcement ratio so that the crack move upward faster reduced the compression region. While on the specimen B-60 and B-40, although the grid has

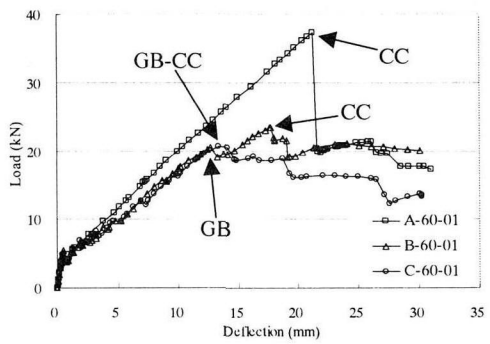

GB : Grid Broken
CC : Crushing of concrete
GB-CC : GB followed soon by CC

(a) Results for type A-60, B-60 and C-60

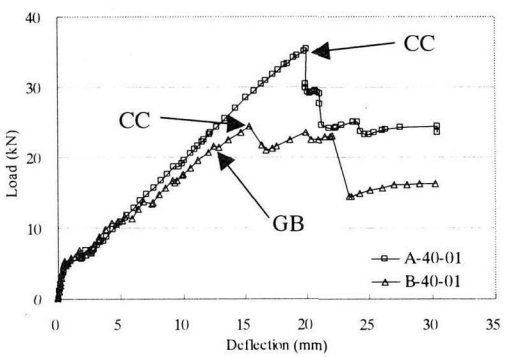

GB : Grid Broken
CC : Crushing of concrete

(b) Results for type A-40 and B-40

Figure 7 Load-deflection relationship

broken or lost its bond capacity, the concrete did not crush soon. The applied load still increased.

From this investigation, the load-deflection relationship of a concrete beam reinforced by UCAS may be divided into three steps, which are, the uncracked step; from zero to first crack, the crack propagating step; from first crack to maximum capacity and the pseudo-ductile behavior which is indicated by rather horizontal load-deflection relationship. Based on this results, the load-deflection response of UCAS beam may be divided into three categories, that are category A, B and C, as illustrated in Figure 8. Category A is the load-deflection mode where the grid does not fail when beam fails under concrete compression failure. This mode is indicated by dropping of load capacity when concrete crushed. Category B is the load-deflection mode where the grid fails earlier followed soon by the crushing of concrete. This mode is indicated with no dropping of load when concrete crush, but the deflection moves with almost no change in load. And category C is load-deflection mode where the crushing of concrete do not occur soon when grid broken. This mode is indicated by a little dropping of load when crushing of concrete. From those categories, the category B is the best load-deflection mode according to the safety consideration. The load-deflection mode of category B can be achieved when the grid broken followed soon by the crushing of concrete.

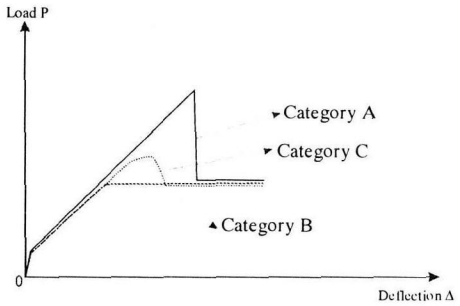

Figure 8 Load-deflection mode of UCAS beam

3.2 Crack pattern and failure mode

Figure 9 shows the load-crack width relationship for specimen A-60 and B-60. Initially, the beam was uncrack. When the stresses at the bottom of the beam reached the tensile strength of the concrete, cracking occurred when applied load reached about 9 kN. From here, the appeared crack opened together with increasing the applied load. P1, P2 and P3 are the gauge name that measure the crack width at three points. The position of crack gauges are marked in Figure 10. The gauges were attached when the crack occurs first time. Only the first three cracks that were

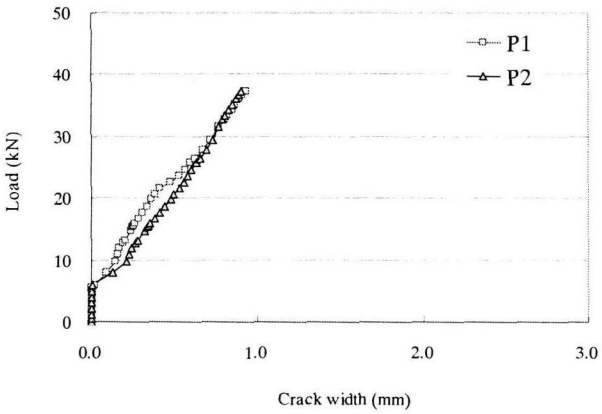

(a) Crack width of A-60

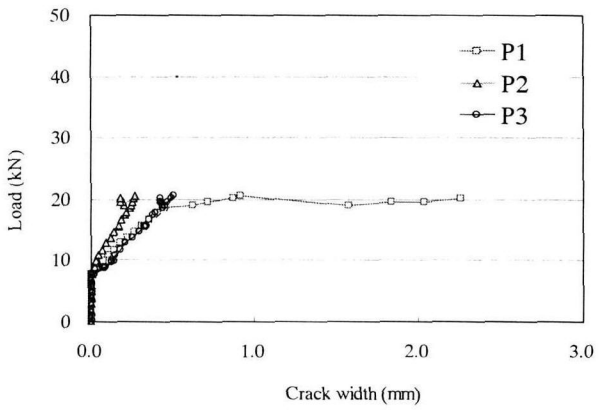

(b) Crack width of B-60

Figure 9 Load-crack width relationship for specimen A-60 and B-60

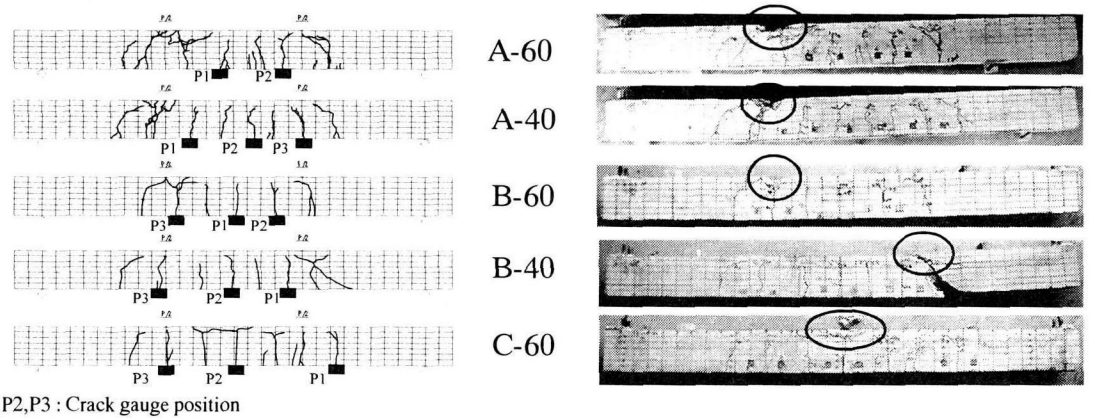

P1,P2,P3 : Crack gauge position

Figure 10 Crack pattern and failure mode photos

measured by crack gauges. All the measured crack were almost within pure bending span. Figure 9 shows that all measured crack propagated uniformly together with increasing of applied load. This is also indicated that the grid system can effectively work to offer a good bonding mechanism between tensile reinforcement and concrete. When the grid on specimen B-40 near the point where the gauge P1 attached failed, the crack on that point opened fast while on the other points (P2 and P3), the cracks closed and did not open again until the end of test. As presented in Figure 9(a), the crack opened up to about 3.5 mm on P1, while the crack just opened up to about 0.5 mm on P2 and P3.

Typical crack pattern and failure mode photographs of the specimen types A, B and C are shown in Figure 10. The existence of grids caused most of the flexural crack to widen and extend slowly upward to the compression face. Crack spacing in the specimen with higher reinforcement ratio was observed to be smaller than the others. The grid failure on the beam types B and C occurred early and this caused a crack to widen and extend fast toward the compression face.

Based on visually investigation, the beams with reinforcement ratio of 0.78% failed under pure compression failure. There was no grid broken that has been identified in this type. While on the specimen with reinforcement ratio of 0.61% and 0.49%, beams failed under grid bond failure which was followed by the crushing of concrete. Based on the results that the load did not drop significantly when grid broken then it was considered that the grid broken under shear failure (slip) on epoxy rein that connects the main and vertical cable. This causes the grid capacity depends on the tensile-shear strength of epoxy resin. The effect grid pitch to the crack spacing could not be identified in this study.

3.3 Strain distribution

Typical strain distribution, both along half of the longitudinal reinforcement and along the height of the beams cross section at center span for A-60 and B-60 are presented in Figure 11. On both specimens, strain distribution results were similar. Initially, the beam was uncrack. In this stage, the strain at tensile reinforcement was still very small. When the stress at the bottom of the beam reached the tensile strength of the concrete, cracking occurred. After cracking, the tensile force in the concrete was transferred to the tensile reinforcement. As a result, the strain in the tensile reinforcement increased. With further loading, the strain increased together with increasing the applied load until the beam reached its maximum capacity.

On tensile reinforcement, at maximum load, strain distributed from approximately zero on F1b to approximately 7000×10^{-6} in strain on F3b and F4b. This strain distribution pattern indicated that the grid-system worked effectively as mechanical bonding between longitudinal reinforcement and concrete. After peak load, the strain around pure bending span decreased. At the end of test, the measured strain on the tensile reinforcement at mid span was approximately 2000×10^{-6} in strain.

On the measured strain distribution along the height of cross section at center span, the strain distribution pattern was also similar for both specimens. The dot represents strain measurement on the reinforcement cables at maximum load. The measured strains at maximum load can be considered linear from concrete compression strain to tensile reinforcement strain. This phenomenon implies that the section are plane before bending remain plain after bending. This is one of the basic assumption in flexural theory [10]. This indicates that there is a good interaction between concrete and reinforcement. The agreement

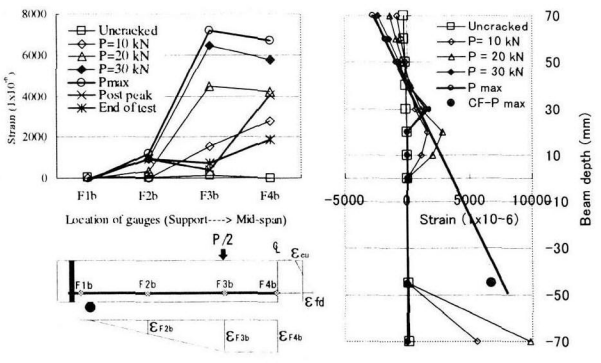

(a) Typical strain distribution for A-60

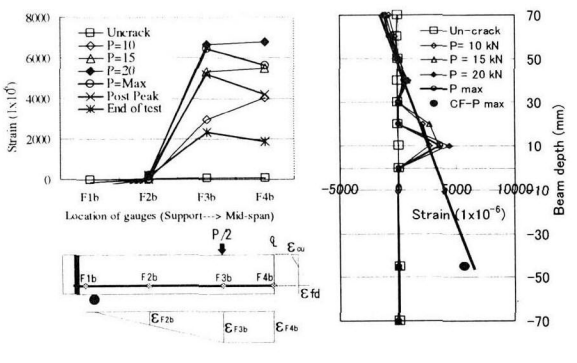

(b) Typical strain distribution for B-60

Figure 11 Strain distribution on cable and mid-span cross section of concrete

Table 3 Reinforcement ratio

Type	Section area factor (S_a)	Balanced reinforcement ratio (%)		Section area (mm2)		Number of turning per cables (N_n) *	Comments
		ρ_b	$\rho_n = \rho_b \times S_a$	A_b	$A_n = A_b \times S_a$		
A	1.5	0.52	0.78	54.6	81.9	22	Over reinforcement
B	1	0.61	0.61	64.1	64.1	17	Balanced reinforcement
C	0.8	0.61	0.49	64.1	51.2	14	Under reinforcement

* Four cables as tensile reinforcement for each beam

Table 4 Load carrying capacity

Type	Specimen name		Theoretical				Experimental		Ratio			Failure mode
			$M^{o}cr$ (kN.m)	S_a	Balanced ($M^{o}u_b$)	Actual ($M^{o}u_a$)*	Mcr (kN·m)	M_{max} (kN·m)	Mcr/$M^{o}cr$	$M_{max}/M^{o}u_b$	$M_{max}/M^{o}u_a$	
A	A-60	1	0.96	1.5	8.47	8.47	0.88	8.39	0.92	0.99	0.99	Comp
		2	0.96		8.47	8.47	0.82	8.61	0.85	1.02	1.02	Comp
		3	0.96		8.47	8.47	0.88	8.34	0.92	0.99	0.99	Comp
	A-40	1	0.96		8.47	8.47	1.10	7.95	1.15	0.94	0.94	Comp
		2	0.96		8.47	8.47	1.10	7.73	1.15	0.91	0.91	Comp
		3	0.96		8.47	8.47	0.88	7.28	0.92	0.86	0.86	Comp
B	B-60	1	1.06	1	9.79	6.88	1.33	5.08	1.25	0.52	0.74	Comp
		2	1.06		9.79	6.88	1.33	5.28	1.25	0.54	0.77	Comp
	B-40	1	1.06		9.79	6.88	1.33	6.67	1.25	0.68	0.97	Comp **
		2	1.06		9.79	6.88	1.22	5.21	1.15	0.53	0.76	Comp
C	C-60	1	1.06	0.8	9.79	5.60	1.10	4.30	1.04	0.44	0.77	Comp
		2	1.06		9.79	5.60	1.33	4.48	1.25	0.46	0.80	Comp

* Calculated with Sa=1.5

** Compression-shear failure

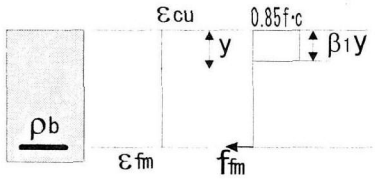

Figure 12 Rectangular stress block

between the strain measured in the reinforcement, plotted with a dot in Figure 11, and the line through the concrete strain curve shows that the tensile reinforcement and concrete do act together as postulated in the basic assumption of flexural theory. This phenomenon occurs only when the grids can develope good mechanical bond. If there is no good bond or grid broken, the strain of reinforcement and concrete at same level will diverge.

3.4 Load carrying capacity

Table 3 presents the balanced reinforcement ratio ρ_b calculated based on the rectangular stress block (Figure 12) assumed for concrete as well as the nominal reinforcement ratio ρ_n according to the section area factor S_a value. The section area factor S_a represents the fact that it is impossible to consider that all carbon fiber filaments can work uniformly when the cables sustaining the tension forces. This is attributed to the natural fact that fibers in a bundle can not be in same initial stress when sustaining the applied tensile load. The slack fiber must be present in a bundled fiber. It should be noticed here that the factor S_a represents the factor of section area at balanced condition. The value of S_a must bigger than one. However, in this study, a value smaller than 1.0 is also taken as a parameter to represent an under reinforced concrete. The S_a value of 1.5, 1.0 and 0.8 are considered in designing the specimen parameters for this study. S_a=1.5 represents an over reinforced concrete beam, S_a=1.0 represents a balanced reinforced concrete beam and S_a=0.8 represents an under reinforced concrete beam. Based on the experimental result, the suitable Sa value would be chosen to recalculate the actual capacity.

By Figure 12, the nominal reinforcement ratio was calculated by multiplying the ρ_b with S_a as expressed by Eq.(1).

$$\rho_n = \frac{0.85\beta_1 f_c'}{f_{fm}}\left(\frac{\varepsilon_{cu}}{\varepsilon_{cu}+\varepsilon_{fm}}\right)S_a \qquad (1)$$

Here, β_1 is equal to 0.8 for concrete with compressive strength f'c up to 50 MPa, and equal to 0.72 for compressive strength f'c higher than 50 MPa [9]. A balanced beam failure was assumed when concrete reaches its ultimate compressive strain (ε_{cu}=0.0035) and UCCF cables reaches their design tensile strain (ε_{fm}=0.0073 at 35% of nominal tensile strength), simultaneously.

In Table 4, the balance moment for each S_a values, actual moment for S_a=1.5 and theoretical crack moment as well as the experimental moment at first crack M_{cr}, and the maximum moment Mmax of specimens are presented. The theoretical M^{o}_{cr} was calculated by Eq.(2), where f_{ct} = tensile strength of concrete, I_g= the moment of inertia of the gross section and y_t=the distance from centroid to extreme tension zone. The moment of inertia of the gross concrete section I_g ignored the small increase in the moment of inertia due to the reinforcement.

$$M^{o}_{cr} = \frac{f_{ct} I_g}{y_t} \qquad (2)$$

From Table 4, the experimental Mmax seems to agree with the predicted balanced moment capacity by using S_a=1.5, where the ratio between Mmax and $M^{o}u_b$ is about 0.95 while it is approximately 40% and 60% smaller in specimen types B and C, respectively. Based on this phenomenon, the value of S_a=1.5 is considered as the suitable value for this case. So, by using S_a=1.5, the actual ultimate moment $M^{o}u_a$ presented in Table 4 may be predicted using Eq.(3), as follows:

$$M^{o}u_a = \left(\frac{A_n}{S_a}\right) f_{fm}\left(d - \frac{a}{2}\right) \qquad (3)$$

where, A_n=nominal section area of reinforcement, S_a=Section area factor=1.5, f_{fm}= maximum tensile strength

Table 5 Bond capacity of grid

Type	Specimen name	Reinforcement position	Number of turning per cables	Dn (mm)	D (mm)	w (mm)	Bond length (mm)	Bond width (mm)	Shear strength of materials (Mpa)*	Bond capacity Pb (kN)
A	A-60	Second layer	22	5.08	9.14	8.56	9.14	18.56	9.8	1.66
		First layer		5.08	9.14	8.56	14.04	18.56	9.8	2.55
	A-40	Second layer	22	5.08	9.14	6.63	9.14	16.63	9.8	1.49
		First layer		5.08	9.14	6.63	14.04	16.63	9.8	2.29
B	B-60	Second layer	17	4.46	8.03	8.56	8.03	18.56	9.8	1.46
		First layer		4.46	8.03	8.56	12.32	18.56	9.8	2.24
	B-40	Second layer	17	4.46	8.03	6.63	8.03	16.63	9.8	1.31
		First layer		4.46	8.03	6.63	12.32	16.63	9.8	2.01
C	C-60	Second layer	14	4.05	7.29	8.56	7.29	18.56	9.8	1.33
		First layer		4.05	7.29	8.56	11.19	18.56	9.8	2.04

*) See Table 2

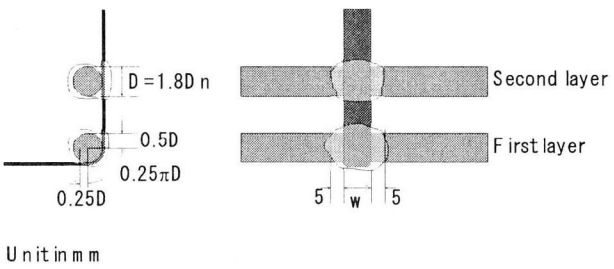

Figure 13 Bond surface of grid

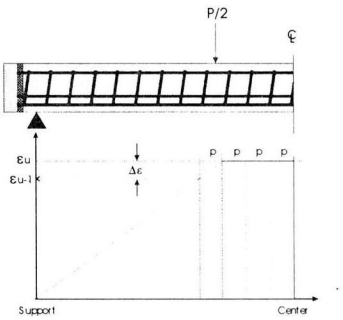

Figure 14 Strain distribution model

of cable, d= effective depth of section, a=depth of rectangular compression stress block assumed for concrete.

Although the specimen type C was designed to fail under cable tension failure it can be observed, through Table 4, that all beams failed in compression. This is may be based on the fact that on the specimen types B and C, the grid failed before concrete reach its concrete strength. As discussed previously, that the failure of grid caused the crack extends fast reducing the compression region of concrete.

Furthermore, Table 4 also shows that Eq.3 with S_a=1.5 agrees well for specimen type A, but still overestimates (about 20% higher than the experimental ultimate moment) for beam types B and C. These differences may be also attributed to the variability of the tensile strength of the UCCF cables, effect of cement paste on cables and bond capacity of grids. As discussed previously, the grid failure for specimen types B and C has been observed and this causes the reduction of maximum capacity of the beams. So based on this phenomenons, the maximum load of specimen types B and C tends to be controlled by the bond capacity of the grid rather than by concrete strength or cable strength.

3.5 Limit Moment (LM)

The grid failure on specimens B and C followed by the crushing of concrete caused the reduction of ultimate moment of concrete beams. This phenomenon caused the maximum capacity of the beam to be controlled by the grid bond capacity.

Figure 13 shows the grid bond surface details. If w (mm) is taken as 5 times the nominal diameter of stirrups then the bonding surface of the grid on the first and second layers of reinforcement may be expressed, respectively as follows:

$$A_{b1} = 1.8D_n(0.75 + 0.25\pi)(w + 10) \quad (4)$$

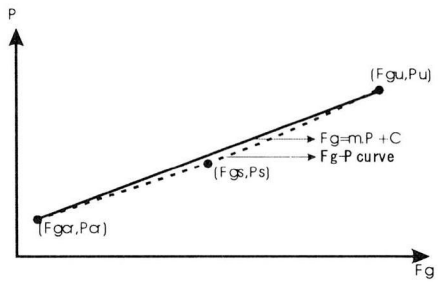

Figure 15 Applied load (P) vs Grid force (Fg)

$$A_{b2} = 1.8D_n(w + 10) \quad (5)$$

where D_n is the nominal diameter of cables calculated based on the section area of fiber filament and w is width of vertical reinforcement. So, the bond capacity may be expressed as follows:

$$P_{b1} = \tau_e . A_{b1} \quad (6)$$

$$P_{b2} = \tau_e . A_{b2} \quad (7)$$

where τe is the shear bond strength of resin and A_{b1} and A_{b2} are bonding surface of grid on first layer cables and bonding surface of grid on second layer cables, respectively. It should be noted here that the adhesive bond of carbon fiber cables was ignored. So, the bond action of cables in UCAS beam is locally bond concentrated on grids. Based on this assumption, the bond capacity depends on the shear capacity of epoxy resin that connect the main cable and vertical reinforcement

In this section, the maximum capacity controlled by

Table 6 Limit moment (LM)

Type	Specimen name	Reinforcement position*	Δε (1x10^{-6})	Fg (kN)	Pb (kN)	P_{LM} (kN)	LM (kN·m)	M°u (kN·m)	Mmax (kN·m)	LM/Mmax	LM/M°u
A	A-60-1	Second layer	836.7	2.65	1.66	24.34	5.48	8.47	8.39	0.65	0.65
		First layer	1111.1	3.52	2.55	27.46	6.18			0.74	0.73
	A-60-2	Second layer	836.7	2.65	1.66	24.34	5.48	8.47	8.61	0.64	0.65
		First layer	1111.1	3.52	2.55	27.46	6.18			0.72	0.73
	A-60-3	Second layer	836.7	2.65	1.66	24.34	5.48	8.47	8.34	0.66	0.65
		First layer	1111.1	3.52	2.55	27.46	6.18			0.74	0.73
	A-40-1	Second layer	557.8	1.77	1.49	31.24	7.03	8.47	7.95	0.88	0.83
		First layer	740.7	2.35	2.29	35.47	7.98			1.00	0.94
	A-40-2	Second layer	557.8	1.77	1.49	31.24	7.03	8.47	7.73	0.91	0.83
		First layer	740.7	2.35	2.29	35.47	7.98			1.03	0.94
	A-40-3	Second layer	557.8	1.77	1.49	31.24	7.03	8.47	7.28	0.97	0.83
		First layer	740.7	2.35	2.29	35.47	7.98			1.10	0.94
B	B-60-1	Second layer	836.7	3.07	1.46	22.61	5.09	6.88	5.08	1.00	0.74
		First layer	1111.1	4.07	2.24	25.38	5.71			1.12	0.83
	B-60-2	Second layer	836.7	3.07	1.46	22.61	5.09	6.88	5.28	0.96	0.74
		First layer	1111.1	4.07	2.24	25.38	5.71			1.08	0.83
	B-40-1	Second layer	557.8	2.04	1.31	28.75	6.47	6.88	6.67	0.97	0.94
		First layer	740.7	2.72	2.01	32.52	7.32			1.10	1.06
	B-40-2	Second layer	557.8	2.04	1.31	28.75	6.47	6.88	5.21	1.24	0.94
		First layer	740.7	2.72	2.01	32.52	7.32			1.40	1.06
C	C-60-1	Second layer	836.7	3.07	1.33	20.53	4.62	5.6	4.3	1.07	0.82
		First layer	1111.1	4.07	2.04	22.97	5.17			1.20	0.92
	C-60-2	Second layer	836.7	3.07	1.33	20.53	4.62	5.60	4.48	1.03	0.82
		First layer	1111.1	4.07	2.04	22.97	5.17			1.15	0.92

*) From bottom

the grid is called the limit moment LM and the maximum capacity controlled by concrete or reinforcement is called the ultimate moment. When the grid controls the maximum capacity of the beam, the beam capacity will be lower than the ultimate capacity.

Table 5 presents the bond capacity P_b of each specimen type. This bond capacity is an important variable in order to develope a good interaction between reinforcement and concrete. The Pb value is used in predicting LM. This significantly influences the maximum capacity of beam. When the grid loss its bond capacity before concrete crush or reinforcement fail, then the maximum capacity of beam will be smaller than the ultimate moment, or it can be said that LM will be smaller than ultimate capacity. In contrary, if grid enough strong so that the grid do not fail until concrete crush then the maximum moment will be same to the ultimate moment. So, LM may be defined as the moment that can be carried by the beam until the grid fails. In predicting LM, it was considered that the grid failed just caused by the forces occurred on main cables. For simplifying, the effect of vertical reinforcement is ignored. This based on the fact that the grid tends to fail under longitudinal slip of main cable rather than the vertical slip of vertical reinforcement. To determine LM, the relationship between applied moment and force that works on grid needs to be determined. Figure 14 shows the diagram model of strain distribution along tensile reinforcement when full bonding condition is assumed. This assumption was based on the fact that the experimental strain distribution presented in Figure 11 closed to the strain distribution for full-bond reinforcing system. By assuming that grid develops full bond mechanism, the force which occurs due to applied load on grid may be defined as deviation of strain on cable between two grids and can be mathematically expressed as:

$$F_g = \frac{A_n}{S_a N_g} \Delta\varepsilon E_{cf} \qquad (8)$$

where A_n is nominal section area of tensile reinforcement, Ng is the number of grids on that section and E_{cf} is Young modulus of carbon fibers. If Fg exceeds Pb then the grid broken.

This F_g must be distributed to the intersection point on first (F_{g1})and second (F_{g2}) layers of cables. If F_{g1} exceeds the P_{b1} (Eq.6) or F_{g2} exceeds P_{b2} (Eq.7), then the grid breaks. LM may be predicted based on the relationship between grid force F_g and applied load as shown in Figure 15. That curve is determined by calculating the F_g at first crack F_{gcr}, service load F_{gs} and ultimate load F_{gu}. To simplify, this curve is approximated with a linear relationship that can be expressed by Eq.9, where P_{LM} is applied load when grid forces equal to F_g, and C and m are curve constants. Then, the limit moment load P_{LM} when grid force equal to F_g can be easily converted to the moment that represents LM.

$$P_{LM} = 1/m\,(F_g - C) \qquad (9)$$

Table 6 presents the grid forces Fg and LM. It can be observed that all beams have smaller LM than ultimate capacity (calculated by Eq.(3)). This result indicates that the maximum moment of beam will be controlled by grid bond capacity. This is also observed when testing. This predicted capacity is in accordance with the experimental results except for specimen A-60 that seems to have higher grid bond capacity than predicted. When the beam has a LM point small enough , then its behavior will be a pseudo-ductile.

4. Conclusion

The results of this investigation led to the following conclusions:

(1) Test results have shown that the flexural behavior of UCAS-concrete beam is good behavior according to

safety considerations because the flexural behavior shows that after peak load, the beam capacity does not fail rapidly but the beam shows a mechanism where the deflection propagates with almost no significant change in load.

(2) Load-deflection mode of UCAS beam may be divided into three categories. Category A: no grid failure when concrete crush, category B: grid broken and followed soon by the crushing of concrete. This mode is indicated by no dropping of load when grid broken. Category C is load-deflection mode where the crushing of concretes do not occur soon when grid broken. This mode is indicated by little dropping of load when concrete crushed.

(3) The existence of grid offers good influence to the flexural behavior where most of the flexural crack widens and extends slowly upward to the compression face.

(4) The measured strains at maximum load shows good agreement with the basic assumption of flexural theory, that the strain in reinforcement is equal to the strain in the concrete at the same level. This assumption implies perfect bond between concrete and reinforcement. This shows that the tensile reinforcement and concrete do act together as postulated in the basic assumption.

(5) The maximum capacity of concrete beam may be controlled by the bond capacity of the grid. When the LM is smaller than ultimate capacity of beam or grid fails earlier, then the capacity of beam tends to be controlled by the grid bond capacity. On the contrary, if LM is higher than ultimate capacity of grid does not fail when concrete crush, then the beam capacity will be controlled by concrete strength or by reinforcement strength.

(6) UCAS-beam that fails under grid bond-failure shows a pseudo-ductile performance. It should be noted here that although the grid fails, the existing of end anchors causes the tensile reinforcement to still sustain the tensile load.

(7) The predicted maximum capacity shows close agreement to the experimental results except the experimental result for specimens A-60 that seems to have a higher grid bond capacity than predicted.

(8) Although the specimens type C have been designed as the under reinforced concrete beams but the beam failed under grid-concrete compression failure. This may be attributed to the fact that the concrete paste behaves as adhesive materials to the cable. As the result, the tensile strength of cables embedded in concrete may be approximately 1.5 times higher than the direct tensile test of unresin carbon fibers cable.

The proposed UCAS method can produce a good prospect for RC construction especially for precast RC construction industry in the future. Based on the roughly economic estimating, the initial cost of this method is about 70% of the conventional RC structure. This caused by the eliminating some process, such as no welding, low maintenance, saving labor and equipment, etc. In addition the life cycle cost of structure reinforced by this method is about 30%-50% of the conventional RC ones, due to the corrosion resistance of carbon fiber material[11]. It is, however, some additional attention must be taken for the cast in site construction where a tension device is needed to tensioning the cables. But, the tension level is not so high as the conventional prestressed RC ones. And so, it may be recommended that the UCAS method can be a good alternative for RC structure.

Acknowledgment

The authors gratefully acknowledge the generosity of TORAY and TOHO RAYON industries of Japan, for supplying the carbon fibers for this study. The authors would also like to thank the research members of graduate school of the intelligent machinery and system, Kyushu University, for their cooperation in the making of UCAS cables.

References

1) T.OHTA, K.YAMAGUCHI, K.HARADA and K.SAMIZO, Fundamental Studies on Mechanical Properties of UCCF cables for UCAS method, *Proceeding of 26th conference on Our World in Concrete & Structure, Singapore*, August 2001, pp.521-526.

2) D.RUDY, Y.KOBAYASHI, T.NAGAHAMA, and T.OHTA, Application of Unresin Continuous Carbon Fibers as Flexural Reinforcement in Concrete Structure, *JCI, Vol.22, No.3*, 2000, pp.283-288.

3) B.BENMOKRANE, O.CHAALLAL, and R.MASMOUDI, Flexural Response of Concrete Beam Reinforced with FRP Reinforcing Bars, *ACI Material Journal*, V-91, No.2. May-June 1995, pp.46-55.

4) R.MASMOUDI, B.BENMOKRANE, and O.CHAALLAL, Cracking behavior of concrete beams reinforced with fiber reinforced plastic rebars, *Can.J.Eng.23*, 1996, pp.1172-1179.

5) M.KAY and M.A.ERKI, Flexural behavior of concrete beams pretensioned with aramid fibre reinforced tendons, *Can. J. Civ. Eng.* 20, 1993, pp.688-695.

6) A.NANNI, Fiber-Reinforced-Plastic (FRP) Reinforcement for concrete structures: Properties and Application, *Elsevier*, 1993, 450pp.

7) A. NANNI, Flexural behavior and design of RC members using FRP reinforcement, *Journal of structural Engineering*, Vol.119, No.11, November 1993, pp.3344-3359.

8) L. H. PEEBLES, Carbon fibers: Formation, Structures, and Properties, *CRC Press*, 1995.

9) Japan Highway bridge association, Specification for Highway bridge Part III: Concrete Bridge Design, 1996, 175pp.

10) JAMES.G.,M.GREGOR, Reinforced Concrete: Mechanics and Design, *Prentice Hall, A Division of Simon & Schuster, Englewood Cliffs, New Jersey*, 1988, 799pp.

11) Toshiaki OHTA, "New concept of concrete structure in IT era and its life cycle assesment", *JSCE*, Vol.86.No.3, March 2001, pp.46-49 (in Japanese).

(Received September 14,2001)